

Structural topology optimization on sound radiation at resonance frequencies in thermal environments

YANG XiongWei & LI YueMing*

State Key Laboratory for Strength and Vibration of Mechanical Structures, School of Aerospace, Xi'an Jiaotong University, Xi'an 710049, China

Received December 8, 2013; accepted May 16, 2014; published online August 18, 2014

Thermal and acoustic environments pose severe challenges to the structural design of hypersonic vehicles. One of them is to find optimal design that exhibits ideal acoustic characteristics in a frequency band, which is discussed in this paper through topology optimization aiming at resonance sound radiation in thermal environments. The sound radiation at resonance frequencies is the main component of response, minimization on which is likely to provide a satisfactory design. A bi-material plate subjected to uniform temperature rise and excited by harmonic loading is studied here. Thermal stress is first evaluated and considered as prestress in the following dynamic analysis; radiated sound power is then calculated through Rayleigh integral. Sensitivity analysis is carried out through adjoint method considering the complicated relationship between stress-induced geometric stiffness and design variables. As the resonance frequency is constantly changing during the optimization, its sensitivity should be considered. It is also noticed that mode switching may occur, so mode tracking technique is employed in this work. Some numerical examples are finally discussed.

topology optimization, thermal environment, radiated sound power, resonance response

PACS number(s): 02.60.Pn, 4340.Dx, 43.40.Rj

Citation: Yang X W, Li Y M. Structural topology optimization on sound radiation at resonance frequencies in thermal environments. *Sci China-Phys Mech Astron*, 2015, 58: 034601, doi: 10.1007/s11433-014-5539-5

<p>A, A_i = area of the structure, element i respectively</p> <p>C = structural damping matrix</p> <p>E = structural elastic modulus</p> <p>\mathbf{E} = vector of structural elastic modulus</p> <p>F = amplitude vector of driving load</p> <p>F_t = equivalent thermal force vector</p> <p>J, J_a = Jacobian value at structural position r, r_a respectively</p> <p>K = structural stiffness matrix</p> <p>K_G = structural geometric stiffness for bending</p> <p>L = transform matrix</p> <p>M = structural mass matrix</p> <p>T_0 = initial temperature</p>	<p>T_{cr} = critical buckling temperature</p> <p>U = amplitude vector of dynamic displacement</p> <p>U_n = transverse component of dynamic displacement amplitude</p> <p>U_t = thermal displacement vector</p> <p>V_C = control volume of design material</p> <p>V_i = artificial volume of element i</p> <p>W = radiated acoustic power</p> <p>W_1, W_2 = acoustic power at 1st, 2nd resonance frequency respectively</p> <p>Z = impedance matrix</p> <p>c = speed of sound in air</p> <p>i, j = element ID</p> <p>j = the imaginary term</p> <p>k = wave number, $k=\omega/c$</p> <p>p = acoustic pressure at structural position r</p>
--	--

*Corresponding author (email: liyueuming@mail.xjtu.edu.cn)

\mathbf{r}, \mathbf{r}_a	=	position on structural surface
v, v_a	=	normal surface velocity at structural position \mathbf{r}, \mathbf{r}_a , respectively
Λ	=	adjoint factor in sensitivity analysis
Φ	=	(buckling) mode shape
Φ_{ref}	=	reference mode shape of interest
Φ_{cur}	=	mode shape of currently modified structure
α	=	structural thermal expansion coefficient
β	=	structural thermal stress coefficient, $\beta=E\alpha$
$\boldsymbol{\beta}$	=	vector of structural thermal stress coefficient
ΔT	=	temperature rise
ζ	=	design variable
ρ, ρ_0	=	density of structural material, air respectively
ω	=	driving circle frequency

1 Introduction

One of the challenges in the design of hypersonic vehicles is the severe thermal-acoustic environments [1]. Elevated thermal load due to aerodynamic heating could induce compressive stresses, which may cause thermal buckling and alter the structural dynamic characteristics. High-intensity acoustic excitation could cause structure failure and payload dysfunction in quite a wide frequency band. As resonance component is rather crucial, associated minimization could be of significance to provide light-weight structures operating in such extreme environments.

Ma and Hagiwara [2,3] carried out sensitivity analysis of coupled structural-acoustic systems in automobile manufacture to reduce vehicle interior noise, calculating the sensitivities of the eigenvalues (eigenvectors) and the frequency response respectively. Belegundu et al. [4] described a general way to minimize sound power of a baffled plate at a fixed single frequency or in a frequency band, which was obtained with Rayleigh integral following a frequency response analysis; the total power in the band was approximated as the sum of the power at each resonant frequency in the band, due to the fact that they contribute most to the total power. Hambric [5] discussed various approximation techniques for broadband acoustic radiated noise design optimization and developed an optimization methodology in which design variables such as shell thickness, material loss factors, and rib stiffener locations could be repeatedly manipulated to find the optimal design which met radiated noise level. Kim and Dong et al. [6] employed sequential FEM and BEM in design sensitivity analysis for structural-acoustic problems with direct differentiation method and adjoint variable method respectively; the structural dynamic behavior was first obtained through frequency response analysis, and BEM was used to solve the pressure response of the acoustic domain.

The application of topology optimization in acoustic design was first carried out by Luo and Gea [7], to study optimal configuration of stiffeners for interior sound reduction

in a coupled structural-acoustic system; the acoustic excitation which fully determines the level of interior sound was chosen as the objective function, and numerical examples were studied under single frequency and a band of low frequency. Lee and Wang et al. [8] employed topology optimization to design holes on a thin-body with genetic algorithms, and the acoustic radiation and scattering was calculated based on normal derivative integral equation. The frequency band from 750 to 850 Hz was decided as a frequency range for the optimization, and the objective was the maximum pressure in the range. Yoon and Jensen et al. [9] carried out a structural-acoustic optimization based on a mixed finite element formulation, in which displacements as well as pressure are the primal variables; it was shown that the mixed elasticity formulation degenerates to the Helmholtz equation thus the response of the acoustic domain can be modeled correctly using this mixed formulation. Du and Olhoff [10,11] studied the topology optimization problems to minimize the sound power or sum of the pressure square radiated from the structural surface(s) into a surrounding acoustic medium, the calculation of which consisted of structural dynamic analysis and subsequent acoustic calculation using simplified Helmholtz integral or empirical formula.

Anti-vibro design often requires a firm junction between the structural surface and the vehicle construction, which may lead to high thermal stresses, when the structure is subjected to severe thermal environments [12]. It is known that compressive thermal stresses may reduce structural stiffness, and then could affect the optimal design; similar problems could also be found in design on buckling resistance, which also needs to deal with the stress-induced geometric stiffness. It has been known (see e.g. ref. [13]) that the relationship between geometric stiffness and design variable is quite complicated, as change of one design variable will alter the whole structural stress field and each elemental geometric stiffness will then vary. Manickarajah et al. [13] applied Evolutionary Structural Optimization (ESO) method for the optimum thickness design to maximize buckling load of a plate with different boundary conditions; it was assumed that the change of geometric stiffness at each optimization step could be neglected provided that the modification to the thickness distribution was kept sufficiently small. Foldager et al. [14] dealt with the optimization of buckling load for laminated composite structures, fully considering the relationship between the geometric stiffness and design variable in a direct way; as there were only several design variables, this direct method was workable. Pedersen [15,16] optimized the static compliance or eigenvalues of prestressed isotropic and laminated plates; sensitivity analysis was deduced with adjoint approach in which the relationship between the geometric stiffness and design variable was also fully considered. The optimization started with constant prestress, indicating an unchanged equivalent prestress-induced force, which leads to certain

difference from optimization with constant temperature rise; the internal stresses and the geometric stiffness were evaluated at each iteration through solution of a static problem. Lund [17] maximized the buckling load factor of laminated composite shell using the Discrete Material Optimization (DMO) approach; the derivate of the geometric stiffness to each design variable was deduced directly but calculated with central difference approximations.

Yang et al. [18] studied radiated sound optimization of a baffled plate excited by a harmonic load with prescribed frequency in thermal environments, in which the relationship between geometric stiffness and design variable was localized at element level for simplicity. Yang et al. [19] then fully considered this relationship through structural dynamic compliance optimization in thermal environments; at each iteration, the thermal stress was first evaluated and then considered as prestress in the following pre-buckling dynamic analysis; the sensitivity analysis was carried out efficiently using adjoint method to deal with a relatively large number of design variables. The thermal-acoustic optimization problem was thereafter revisited in ref. [20].

Literature survey shows that structural-acoustic optimization in a frequency band has always been a topic of interest. Generally, there are two ways to estimate the dynamic response in a frequency band, i.e. integration of the dynamic response in the band [7], and approximation by the main dynamic component in the band [4,8]. This work carries out such an investigation in thermal environments through minimization of sound radiation at resonance frequencies; it was supposed and finally proved that minimization of radiated sound power at resonance frequency could improve the acoustic characteristics in the nearby band. The main difference from previous work in ref. [20] is that this work focuses on radiated sound power at resonance frequency other than prescribed frequency. During the optimization, the resonance frequency is constantly changing and mode switching may occur; thus mode tracking technique is employed to ensure a smooth convergence. It is assumed that the resonance frequency is the natural frequency as long as this mode is excited.

Recently Yang et al. [21] presented a paper on structural optimization against dynamic compliance at resonance frequencies in thermal environments; comparison with present work may reveal some phenomenon when it comes to dynamic optimization involving resonance.

2 Optimization problem

2.1 Dynamic structure in thermal environment

When a plate is subjected to temperature rise from the ambient, thermal stress develops which may change the structural stiffness and even induce buckling. The structural dynamic FE equation in the pre-buckling state can be written

in a linear stress-stiffening form [22]:

$$(\mathbf{K} + \mathbf{K}_G - \omega^2 \mathbf{M}) \boldsymbol{\Phi} = \mathbf{0}, \quad (1)$$

$$(\mathbf{K} + \mathbf{K}_G + j\omega \mathbf{C} - \omega^2 \mathbf{M}) \mathbf{U} = \mathbf{F}. \quad (2)$$

At resonance frequencies, determinant of the dynamic stiffness $(\mathbf{K} + \mathbf{K}_G - \omega^2 \mathbf{M})$ equals zero; thus, damping is considered in eq. (2) to calculate resonance response.

The geometric stiffness for bending \mathbf{K}_G is induced by in-plane thermal stresses which can be obtained with thermal displacement \mathbf{U}_t :

$$\mathbf{K} \mathbf{U}_t = \mathbf{F}_t. \quad (3)$$

Note that stiffness \mathbf{K} is only related to elastic modulus E while thermal force \mathbf{F}_t to both elastic modulus E and thermal expansion α , so the thermal stress coefficient $\beta = E\alpha$ is introduced to avoid incompatibility that may occur between the stiffness \mathbf{K} and the thermal load \mathbf{F}_t in the material interpolation model [19,23]. It can be found that \mathbf{K}_G is also the function of β , since part of the membrane stress is directly induced by thermal expansion.

2.2 Finite element discretization for radiated power

Consider a vibrating plate mounted on a rigid baffle and placed in a light fluid such as air. With the velocity v_a at point \mathbf{r}_a , the pressure p at point \mathbf{r} can be described through Rayleigh integral; then the acoustic power W radiated from the vibrating plate can be written as:

$$W = \int_A \frac{1}{2} \text{Re}(pv^*) dA = \frac{\rho_0 \omega}{4\pi} \int_A \int_A v_a \frac{\sin(k|\mathbf{r} - \mathbf{r}_a|)}{|\mathbf{r} - \mathbf{r}_a|} dA v^* dA, \quad (4)$$

where *(asterisk) indicates complex conjugation of the quantity. Note that $\sin(k|\mathbf{r} - \mathbf{r}_a|)/|\mathbf{r} - \mathbf{r}_a|$ approaches k when $\mathbf{r} = \mathbf{r}_a$. Eq. (4) can be restated in FE form using the transverse component of displacement \mathbf{U}_n ,

$$W = \frac{\rho_0 \omega}{4\pi} \sum \sum v_a^T J_a \frac{\sin(k|\mathbf{r} - \mathbf{r}_a|)}{|\mathbf{r} - \mathbf{r}_a|} J v^* = \mathbf{U}_n^* \mathbf{Z} \mathbf{U}_n. \quad (5)$$

Note that single point Gaussian quadrature is used, which is accurate enough for current work; v_a , v are then the normal velocity at the centroids (\mathbf{r}_a and \mathbf{r}) of element. Readers can refer to Belegundu et al. [4] for details.

2.3 Mode tracking

Mode switching may occur during the optimization involving natural frequencies [24]. If the optimization is carried out regardless of mode switching, convergence will possibly be deteriorated. Thus, mode tracking technique is adopted to ensure the optimization to be carried out smoothly.

MAC (Modal Assurance Criteria) proposed by Ewins [25] is adopted here

$$\text{MAC} = \frac{\{\Phi_{\text{ref}}^T \cdot \Phi_{\text{cur}}\}^2}{\{\Phi_{\text{ref}}^T \cdot \Phi_{\text{ref}}\} \{\Phi_{\text{cur}}^T \cdot \Phi_{\text{cur}}\}}. \quad (6)$$

In eq. (6), Φ_{cur} denotes the mode shape of reference, associated with the resonance frequency of interest; Φ_{ref} refers to the mode shape of the current structure. MAC varies between 0 and 1; when it equals 1, the vector Φ_{cur} is identical to Φ_{ref} ; when the two vectors are orthogonal to each other, MAC equals 0. Generally the two vectors cannot be the same, and the mode with the highest MAC is identified as the targeted one.

3 Optimization formula

The topology optimization problem for minimizing the radiated sound power at resonance frequency of the bi-material plate in the thermal environment can be stated as:

$$\begin{aligned} \min W &= \mathbf{U}_n^* \mathbf{Z} \mathbf{U}_n, \\ \text{s.t. } (\mathbf{K} + \mathbf{K}_G + j\omega\mathbf{C} - \omega^2\mathbf{M})\mathbf{U} &= \mathbf{F}, \\ (\mathbf{K} + \mathbf{K}_G - \omega^2\mathbf{M})\Phi &= \mathbf{0}, \\ \mathbf{K}\mathbf{U}_i &= \mathbf{F}_i, \\ \sum_i V_i \zeta_i &\leq V_C, \\ \zeta_i &\in (0,1). \end{aligned} \quad (7)$$

At each iteration, the 3rd constraint equation is solved to calculate the displacement \mathbf{U}_i firstly to establish the geometric stiffness matrix \mathbf{K}_G . Secondly, modal analysis in thermal environments is carried out through the 2nd constraint equation; mode tracking procedure could be called here if mode switching occurs. Thirdly, frequency response in thermal environments is evaluated with the 1st constraint equation, with which the radiated sound power at resonance frequency can be calculated.

The main difference from the optimization equation in Yang et al. [20] is that ω refers to the resonance circle frequency, identified through the mode extraction analysis and the mode tracking technique. Thus, there are now two factors, i.e. resonance displacement and resonance frequency that need to be considered in objective calculation and sensitivity analysis.

If it is the total radiated power over a band of frequencies to be minimized, the objective function could be stated as the sum of the power at each resonance frequency in the band. Supposing there are two resonance frequencies, one has

$$W = W_1 + W_2. \quad (8)$$

4 Sensitivity analysis

Considering radiated sound power at single resonance frequency, the sensitivity of the objective function W can be written as:

$$\frac{dW}{d\zeta_i} = 2\mathbf{U}_n^* \mathbf{Z} \frac{d\mathbf{U}_n}{d\zeta_i} + \mathbf{U}_n^* \frac{d\mathbf{Z}}{d\zeta_i} \mathbf{U}_n. \quad (9)$$

The derivative of \mathbf{U} can be obtained by differentiating eq. (2); note that the resonance circle frequency is constantly changing during the optimization, derivative of which should also be considered

$$\begin{aligned} &(\mathbf{K} + \mathbf{K}_G - \omega^2\mathbf{M}) \frac{d\mathbf{U}}{d\zeta_i} \\ &= -\left(\frac{d\mathbf{K}}{d\zeta_i} + \frac{d\mathbf{K}_G}{d\zeta_i} - \omega^2 \frac{d\mathbf{M}}{d\zeta_i} - \frac{d\omega^2}{d\zeta_i} \mathbf{M} \right) \mathbf{U}. \end{aligned} \quad (10)$$

In eq. (10), damping is neglected here for the sake of brevity and simplicity. The derivative (or sensitivity) of the resonance circle frequency can be calculated through

$$\frac{d\omega^2}{d\zeta_i} = \Phi^T \left(\frac{d\mathbf{K}}{d\zeta_i} + \frac{d\mathbf{K}_G}{d\zeta_i} - \omega^2 \frac{d\mathbf{M}}{d\zeta_i} \right) \Phi. \quad (11)$$

Note that eq. (11) is about the sensitivity of simple natural frequency. For multiple cases, the problem of non-differentiability could emerge which needs to be dealt with certain special technique [26]. A simplified way is employed in this work by taking average of sensitivities of multiple natural frequencies [27].

It can be found in eq. (5) that the impedance matrix \mathbf{Z} is function of ω , and its derivative is also considered in sensitivity of the objective function eq. (9).

The derivatives of \mathbf{K} and \mathbf{M} in eqs. (10) and (11) can be actually written as $\partial\mathbf{K}_i/\partial\zeta_i$ and $\partial\mathbf{M}_i/\partial\zeta_i$, since the design variable ζ_i denotes the artificial material fraction of element i , indicating that it only affects the material property of element i .

Special attention should be paid to the derivative of geometric stiffness \mathbf{K}_G . With the change of one design variable, \mathbf{K}_G of all the elements will vary, since the thermal displacement field of the whole structure has been altered. Thus, eqs. (10) and (11) can be rewritten as follows:

$$\begin{aligned} &(\mathbf{K}_i + \mathbf{K}_{Gi} - \omega^2\mathbf{M}_i) \frac{d\mathbf{U}_i}{d\zeta_i} \\ &= -\left(\frac{d\mathbf{K}_i}{d\zeta_i} - \omega^2 \frac{d\mathbf{M}_i}{d\zeta_i} - \frac{d\omega^2}{d\zeta_i} \mathbf{M}_i \right) \mathbf{U}_i - \sum_j \frac{d\mathbf{K}_{Gj}}{d\zeta_i} \mathbf{U}_j, \end{aligned} \quad (12)$$

$$\frac{d\omega^2}{d\zeta_i} = \Phi_i^T \left(\frac{d\mathbf{K}_i}{d\zeta_i} - \omega^2 \frac{d\mathbf{M}_i}{d\zeta_i} \right) \Phi_i + \sum_j \Phi_j^T \frac{d\mathbf{K}_{Gj}}{d\zeta_i} \Phi_j. \quad (13)$$

The derivatives of \mathbf{K} , \mathbf{K}_G and \mathbf{M} in eqs. (12) and (13)

could be found in Yang and Li [19], which are omitted here for the sake of brevity. It has been shown that the direct method to obtain derivative of \mathbf{K}_G may consume prohibitively large computational resources mainly due to the massive calculation of derivative of thermal displacement \mathbf{U}_t to design variable ζ_i at each iteration; therefore, the adjoint method is employed in this work to avoid the calculation of derivative of \mathbf{U}_t [14,19].

4.1 Sensitivity of resonance circle frequency

Pedersen [15] firstly carried out sensitivity analysis on resonance (natural) circle frequency through adjoint method, which is briefly presented here in a simpler way for the sake of completeness, as it is quite an important part in the sensitivity analysis of the objective function.

The sensitivity of (simple) natural circle frequency $d\omega^2/d\zeta_i$ is augmented with the differentiation of eq. (3) by introducing an adjoint factor Λ_0 ,

$$\begin{aligned} \frac{d\omega^2}{d\zeta_i} = & \Phi^T \left(\frac{d\mathbf{K}}{d\zeta_i} + \frac{d\mathbf{K}_G}{d\zeta_i} - \omega^2 \frac{d\mathbf{M}}{d\zeta_i} \right) \Phi \\ & + \Lambda_0^T \left(\mathbf{K} \frac{d\mathbf{U}_t}{d\zeta_i} + \frac{d\mathbf{K}}{d\zeta_i} \mathbf{U}_t - \frac{d\mathbf{F}_t}{d\zeta_i} \right). \end{aligned} \quad (14)$$

Note that the differentiation of eq. (3) equals zero; thus the adjoint factor Λ_0 could be arbitrary and this augmentation changes nothing. The geometric stiffness \mathbf{K}_G is the function of thermal displacement \mathbf{U}_t , as well as material property E, β , so eq. (14) can be written as:

$$\begin{aligned} \frac{d\omega^2}{d\zeta_i} = & \Phi^T \left(\frac{d\mathbf{K}}{d\zeta_i} + \frac{\partial \mathbf{K}_G}{\partial E} \frac{\partial E}{\partial \zeta_i} + \frac{\partial \mathbf{K}_G}{\partial \beta} \frac{\partial \beta}{\partial \zeta_i} - \omega^2 \frac{d\mathbf{M}}{d\zeta_i} \right) \Phi \\ & + \Lambda_0^T \left(\frac{d\mathbf{K}}{d\zeta_i} \mathbf{U}_t - \frac{d\mathbf{F}_t}{d\zeta_i} \right) \\ & + \Phi^T \left(\frac{\partial \mathbf{K}_G}{\partial \mathbf{U}_t} \right)^T \frac{\partial \mathbf{U}_t}{\partial \zeta_i} \Phi + \Lambda_0^T \mathbf{K} \frac{d\mathbf{U}_t}{d\zeta_i}. \end{aligned} \quad (15)$$

As it is arbitrary, the adjoint factor Λ_0 could be set to a specific value so that the relating terms involving the derivatives of \mathbf{U}_t could be zero, and then the derivatives of \mathbf{U}_t could be avoided:

$$\Phi^T \left(\frac{\partial \mathbf{K}_G}{\partial \mathbf{U}_t} \right)^T \frac{\partial \mathbf{U}_t}{\partial \zeta_i} \Phi + \Lambda_0^T \mathbf{K} \frac{d\mathbf{U}_t}{d\zeta_i} = \mathbf{0}, \quad (16)$$

through which an adjoint equation can be obtained to calculate factor Λ_0 [19]:

$$\mathbf{K} \Lambda_0 = -\Phi^T \left(\frac{\partial \mathbf{K}_G}{\partial \mathbf{U}_t} \right) \Phi. \quad (17)$$

As mentioned earlier, the design variable ζ_i only affects

the material property of element i , so $\partial E_j/\partial \zeta_i, \partial \beta_j/\partial \zeta_i, d\mathbf{K}_j/d\zeta_i, d\mathbf{M}_j/d\zeta_i, d\mathbf{F}_{ij}/d\zeta_i$ equal 0 when $j \neq i$; eq. (15) has the following form at element level:

$$\begin{aligned} \frac{d\omega^2}{d\zeta_i} = & \Phi_i^T \left(\frac{d\mathbf{K}_i}{d\zeta_i} + \frac{\partial \mathbf{K}_{Gi}}{\partial E_i} \frac{\partial E_i}{\partial \zeta_i} + \frac{\partial \mathbf{K}_{Gi}}{\partial \beta_i} \frac{\partial \beta_i}{\partial \zeta_i} - \omega^2 \frac{d\mathbf{M}_i}{d\zeta_i} \right) \Phi_i \\ & + \Lambda_{0i}^T \left(\frac{d\mathbf{K}_i}{d\zeta_i} \mathbf{U}_{ui} - \frac{d\mathbf{F}_{ui}}{d\zeta_i} \right). \end{aligned} \quad (18)$$

Since all the derivatives in eq. (18) are at element level, they can be easily calculated based on material interpolation model; the sensitivity of natural circle frequency can then be obtained.

4.2 Sensitivity of radiated sound power

The sensitivity in eq. (9) can be augmented with differentiations of eqs. (2) and (3) by introducing adjoint factors Λ_1 and Λ_2 ,

$$\begin{aligned} \frac{dW}{d\zeta_i} = & \mathbf{U}_n^* \frac{d\mathbf{Z}}{d\zeta_i} \mathbf{U}_n + 2\mathbf{U}_n^* \mathbf{Z} \frac{d\mathbf{U}_n}{d\zeta_i} \\ & + \Lambda_1^T \left((\mathbf{K} + \mathbf{K}_G - \omega^2 \mathbf{M}) \frac{d\mathbf{U}}{d\zeta_i} \right. \\ & \left. + \left(\frac{d\mathbf{K}}{d\zeta_i} + \frac{d\mathbf{K}_G}{d\zeta_i} - \omega^2 \frac{d\mathbf{M}}{d\zeta_i} - \frac{d\omega^2}{d\zeta_i} \mathbf{M} \right) \mathbf{U} \right) \\ & + \Lambda_2^T \left(\frac{d\mathbf{K}}{d\zeta_i} \mathbf{U}_t + \mathbf{K} \frac{d\mathbf{U}_t}{d\zeta_i} - \frac{d\mathbf{F}_t}{d\zeta_i} \right). \end{aligned} \quad (19)$$

For the sake of avoiding the derivatives of \mathbf{U} and \mathbf{U}_t , the relating items should be set to zero, through which the following equations could be obtained to calculate the factors Λ_1 and Λ_2 ,

$$(\mathbf{K} + \mathbf{K}_G - \omega^2 \mathbf{M}) \Lambda_1 = -2(\mathbf{U}_n^* \mathbf{ZL})^T, \quad (20)$$

$$\mathbf{K} \Lambda_2 = -\mathbf{U}^T \frac{\partial \mathbf{K}_G}{\partial \mathbf{U}_t} \Lambda_1, \quad (21)$$

where \mathbf{L} is a transforming matrix describing the relationship between \mathbf{U}_n and \mathbf{U} . Similar to eq. (14), eq. (19) can then be written at element level:

$$\begin{aligned} \frac{dW}{d\zeta_i} = & \Lambda_{1i}^T \left(\frac{d\mathbf{K}_i}{d\zeta_i} + \frac{\partial \mathbf{K}_{Gi}}{\partial E_i} \frac{\partial E_i}{\partial \zeta_i} + \frac{\partial \mathbf{K}_{Gi}}{\partial \beta_i} \frac{\partial \beta_i}{\partial \zeta_i} \right. \\ & \left. - \omega^2 \frac{d\mathbf{M}_i}{d\zeta_i} - \frac{d\omega^2}{d\zeta_i} \mathbf{M}_i \right) \mathbf{U}_i \\ & + \Lambda_{2i}^T \left(\frac{d\mathbf{K}_i}{d\zeta_i} \mathbf{U}_{ui} - \frac{d\mathbf{F}_{ui}}{d\zeta_i} \right) + \mathbf{U}_n^* \frac{d\mathbf{Z}}{d\zeta_i} \mathbf{U}_n. \end{aligned} \quad (22)$$

With the adjoint method, three equations, i.e. eqs. (17), (20), (21) need to be solved during the sensitivity analysis at

each iteration, and the sensitivity can be carried out quite efficiently.

As for the radiated sound power in a band described in eq. (8), the sensitivity can be written as follows:

$$\frac{dW}{d\zeta_i} = \frac{dW_1}{d\zeta_i} + \frac{dW_2}{d\zeta_i}. \quad (23)$$

5 Numerical examples

A bi-material plate with dimension 1 m×1 m×0.02 m is studied with material properties as follows:

$$E^{(0)} = 70 \text{ GPa}, \rho^{(0)} = 2650 \text{ kg/m}^3, \alpha^{(0)} = 1.5 \times 10^{-5} \text{ } ^\circ\text{C}^{-1},$$

$$E^{(1)} = 210 \text{ GPa}, \rho^{(1)} = 6500 \text{ kg/m}^3, \alpha^{(1)} = 1.1 \times 10^{-5} \text{ } ^\circ\text{C}^{-1}.$$

And the problem is to find the optimal distribution of the stiffer material, that is, material 1, volume fraction of which is up to 50%. The initial value of all the design variables is set to $\zeta_i = 0.5$.

The plate is meshed with 40×40 isoparametric 4-node elements, and there are 1600 design variables.

The plate is four-edge clamped and subjected to a uniform temperature rise ΔT with $T_0 = 0^\circ\text{C}$ with a unit concentrated force applied normally at the quarter point (0.25, 0.75), illustrated in Figure 1.

Radiated Sound Power Level (SPL, with reference 10^{-12} watts) to the air is calculated with constant mass density of the fluid (i.e. air) $\rho_0 = 1.21 \text{ kg/m}^3$ and sound speed $c = 343.4 \text{ m/s}$.

GCMMA (Globally Convergent version of Method of Moving Asymptotes) algorithm [28] is employed, and the penalty factor 3 is used in the RAMP (Rational Approximation of Material Properties) material interpolation model [29]. Rayleigh damping $C=0.01(K+K_G)$ is considered.

Figure 2 is flow chart of the optimization strategy, showing all key steps in the present work. The left part is about the main procedures and the right part shows some subprocedures.

During numerical investigations, buckling and mode analysis is first carried out to choose the thermal environ-

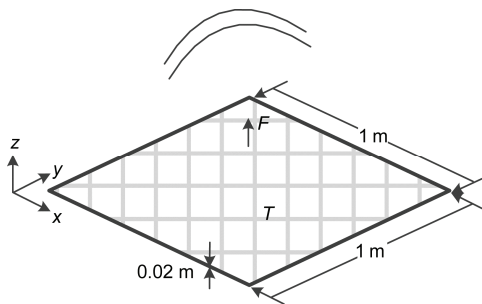


Figure 1 Four-edge clamped plate subjected to a uniform temperature rise with a unit concentrated force applied normally at the quarter point.

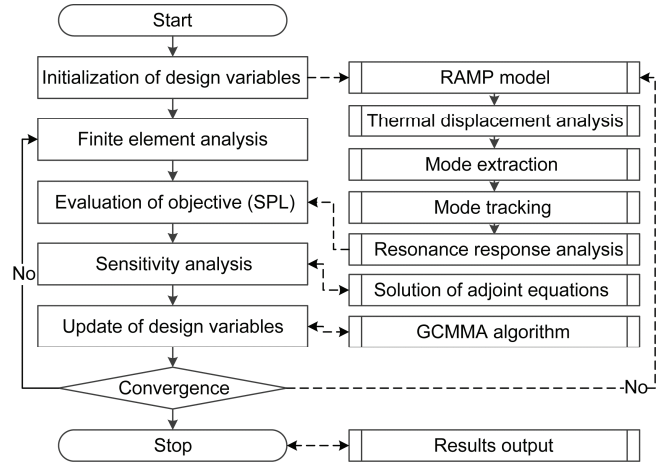


Figure 2 Flow chart of the optimization strategy.

ments and resonance frequencies of interest (i.e. $\Delta T = 0, 50, 75, 90^\circ\text{C}$, and the 1st, 2nd, 13th initial natural frequencies); then the radiated SPL at each resonance frequency under different thermal environments is studied to improve the acoustic characteristics in nearby frequency bands, and sum of the power at the first two resonance frequencies is also investigated.

5.1 Buckling analysis and mode extraction

As the optimization is conducted in the pre-buckling state, thermal environments are chosen below the critical buckling temperature T_{cr} , which can be obtained through an eigenvalue buckling analysis:

$$(K + \lambda K_G) \Phi = 0 \quad (24)$$

in which K_G is evaluated according to the thermal stress induced by temperature change ΔT .

With $T_0 = 0^\circ\text{C}$, the product of λ and ΔT yields $T_{cr} = 100.8^\circ\text{C}$; thus four thermal cases, i.e. $\Delta T = 0, 50, 75, 90^\circ\text{C}$, are investigated in this work.

Modal analysis is then carried out to obtain the modes of interest. It is known that the natural mode may not be a resonance one if it is not excited, which can be checked through orthogonality test or frequency response analysis. The concentrated force is applied at the quarter point (0.25, 0.75) of the plate, and three resonance modes can be identified, i.e. the 1st, 2nd and 13th natural modes of the initial structure.

The 1st is the fundamental mode, the response at which is often the most important component in dynamic response; the 2nd is a multiple mode with the 3rd one; the 13th is a relatively high-order mode, the frequency of which is quite near to that of the 12th. The mode frequencies are shown in Table 1. It can be found that the natural frequencies decrease as the temperature rises, indicating softening effect of the thermal environment. The mode shapes are shown in Figure

Table 1 Natural frequencies in different thermal environments (Hz)

ΔT (°C)	1 st	2 nd	3 rd	12 th	13 th
0	184.1	375.1	375.1	1233	1239
50	131.8	319.0	319.0	1173	1179
75	94.42	286.5	286.5	1141	1148
90	61.34	265.0	265.0	1122	1129

3. As the thermal environment hardly changes the mode shape of this square plate, only the mode shapes with $\Delta T = 0^\circ\text{C}$ are presented.

5.2 Optimization on SPL at the 1st or 2nd initial resonance frequency

Optimization on SPL at the 1st or 2nd initial resonance frequency is supposed to improve the acoustic characteristic in the nearby frequency band where dynamic response is mainly determined by each resonance mode.

Figure 4 shows the optimal topology at the 1st initial resonance frequency. Note that no filtering technique is employed in this work and there are few “gray” elements. As the temperature rises, some stiffer material (i.e. material 1) moves to the margin and the central part becomes smaller.

The load is applied at the up-left quarter-point (0.25, 0.75) of the plate; despite of this, the optimal topology is basically symmetrical, except a little more material 1 at (or around) the location of the load.

Figure 5 shows the optimal topology at the 2nd initial resonance frequency. The topology is symmetrical along the diagonals, which changes slightly as the temperature rises; some stiffer material (material 1) joints the two central parts together.

Note that the materials are isolated, which makes the configuration hard to manufacture; this optimization strategy could be extended to thickness distribution design with minor modification, when the manufacture would not be an issue.

From the comparison between the modes shapes (Figure 3) and the optimal topology (Figures 4 and 5), it could be described that the material mainly lumps according to the mode shapes; this is reasonable as modes shape denotes a pattern of vibration when the structure is driven under the associated frequency. Therefore, it could be concluded that the mode determines the optimal topology, provided that it is excited.

It is noticed that optimal topology is quite similar to that in the published work [21] by the authors, which is on optimization against resonance dynamic compliance in

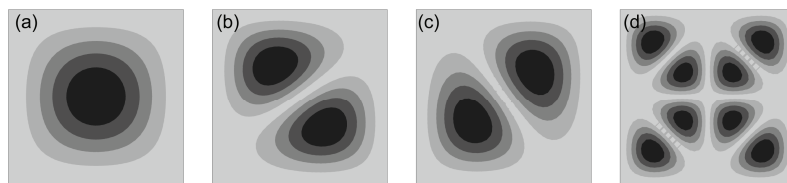


Figure 3 Mode shapes with $\Delta T = 0^\circ\text{C}$. (a) 1st; (b) 2nd; (c) 3rd; (d) 13th.

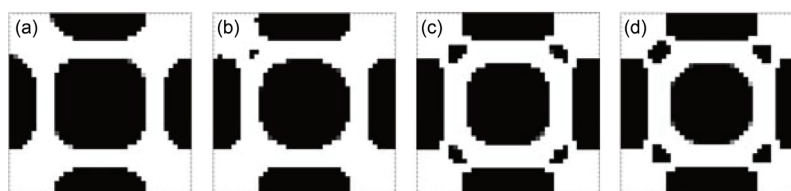


Figure 4 Optimal topology at the 1st initial resonance frequency (white - material 0, black- material 1). (a) $\Delta T = 0^\circ\text{C}$; (b) $\Delta T = 50^\circ\text{C}$; (c) $\Delta T = 75^\circ\text{C}$; (d) $\Delta T = 90^\circ\text{C}$.

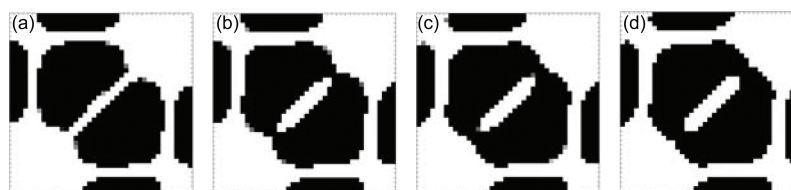


Figure 5 Optimal topology at the 2nd initial resonance frequency (white - material 0, black- material 1). (a) $\Delta T = 0^\circ\text{C}$; (b) $\Delta T = 50^\circ\text{C}$; (c) $\Delta T = 75^\circ\text{C}$; (d) $\Delta T = 90^\circ\text{C}$.

thermal environments. As stated earlier, the mode mainly determines the topology; thus, such similarity is quite reasonable. However, the optimization at the prescribed frequency on dynamic compliance [19] and radiated sound power [20] yields quite different optimal topology. The dynamic compliance describes work of the external load, while the radiated sound power measures a level of energy transfer to infinity.

Figures 6(a) and (b) show the iteration history of the radiated SPL at the 1st and the 2nd resonance frequencies. It can be found that the SPL decreases as the iteration grows, suggesting that the optimization yields designs with ideal acoustic characteristics.

Figures 7(a) and (b) show the iteration history of the 1st and the 2nd resonance frequencies, which increases as the iteration accumulates, suggesting that the structure becomes

stiffer.

It can be found in Figure 6 that the SPL of the initial structure does not change obviously in different thermal environments. Eqs. (4) and (5) suggest that there are mainly two factors contributing to the resonance SPL, the resonance frequency ω and the amplitude of dynamic displacement U . ω decreases as the temperature rises, and so does the Rayleigh damping C which could lead to the increase of U . The effect of these two variations on SPL tends to be at odds, leading to an unobvious change of SPL.

The phenomenon that thermal environment does not exert obvious effect on the resonance radiated SPL is particular to this problem, where a square plate subjected to a uniform temperature is studied with damping $C=0.01(K+K_G)$.

Figures 8(a) and (b) show the iteration history of the critical buckling temperature during the optimization at the

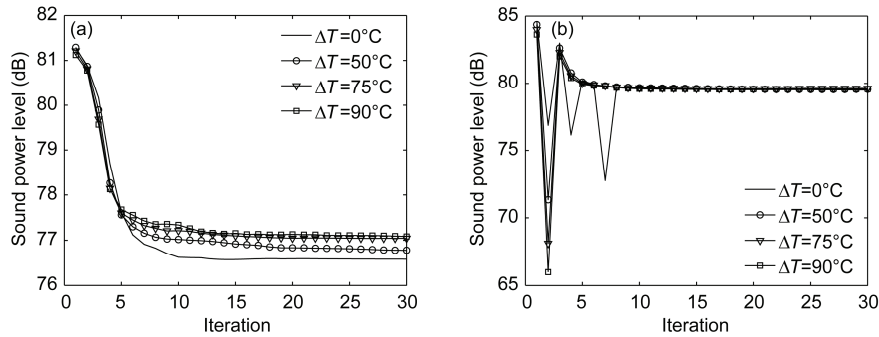


Figure 6 Iteration history of the radiated SPL. (a) 1st initial resonance frequency; (b) 2nd initial resonance frequency.

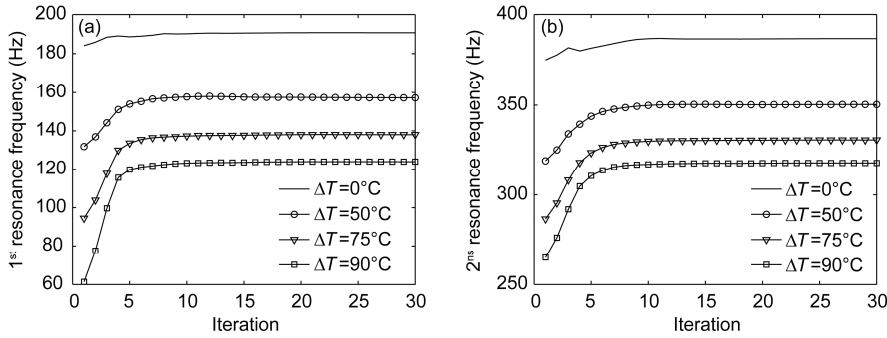


Figure 7 Iteration history of the initial resonance frequencies. (a) 1st initial resonance frequency; (b) 2nd initial resonance frequency.

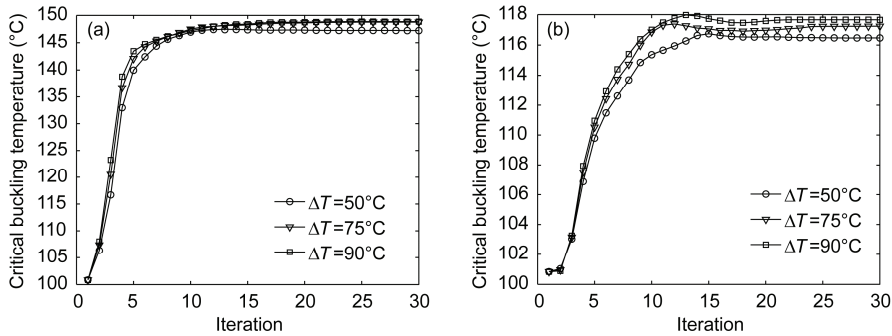


Figure 8 Iteration history of the critical buckling temperature during the optimization. (a) 1st initial resonance frequency; (b) 2nd initial resonance frequency.

1st and the 2nd initial resonance frequencies respectively. T_{cr} increases as the iteration accumulates, and the plate is always in the pre-buckling state.

Mode switching occurs during the optimization at the initial 2nd resonance frequency, as shown in Figure 9. The 2nd resonance mode of the initial structure finally becomes the 3rd one in the optimal design.

It can be found in Figure 9 that the 2nd and 3rd resonance frequencies become unidentical in the optimal design, which subsequently raises an issue that the SPL at the initial multiple frequency may need to be stated as the sum of SPL at two frequencies in the optimal design. However, it can be found from Figure 12 that the initial 3rd natural mode remains unexcited in optimal designs.

5.3 Optimization on the sum of SPL at the 1st and 2nd initial resonance frequencies

Optimization on this is supposed to improve the acoustic characteristics in the frequency range where both the 1st and 2nd modes dominate the dynamic response; comparison with the results obtained in the previous subsection could demonstrate the effect of different objective functions on the optimal designs.

Figure 10 shows the optimal topology in different thermal environments; the topology is kind of similar to that obtained at the 1st resonance frequency except that it is now symmetrical with diagonals, like the topology obtained at 2nd resonance frequency.

Figure 11(a) shows the iteration history of the sum of radiated SPL at the 1st and 2nd initial frequencies; it can be found the radiated SPL of the final design is higher than that

of the initial structure. This does not mean that the final topology is not optimal; note that the initial structure just numerically exists under most circumstances, although it could be possibly manufactured by constructing composites materials with microstructures [30]. It is also noticed that the radiated SPL in different thermal environments is almost the same.

Figure 11(b) shows the iteration history of the buckling temperature, which increases as the optimization proceeds.

Figures 12(a) and (b) shows the radiated SPL in 0–500 Hz of the initial and the optimal structures, wherein the dash-dotted lines mark the resonance frequencies; note that the peak frequencies are not the resonance frequencies. It could be found that the optimization at the 1st (or 2nd) initial resonance frequency yields optimal acoustic characteristics in the associated frequency band, and also leads to some improvement in the band around the 2nd (or 1st) initial resonance frequency.

For the thermal case $\Delta T = 0^\circ\text{C}$ shown in Figure 12(a), the optimization at the 1st initial resonance frequency increases the 1st resonance frequency as well as the 2nd one, while the optimization at the 2nd increases the 2nd resonance frequency but decreases the 1st one. Published work [10] shows that optimization problems against noise can be achieved by driving the structural natural frequencies far away from an external driving frequency or a band of driving frequencies; thus, maximization of natural frequencies or gaps between natural frequencies are often chosen as objectives.

For the thermal case $\Delta T = 90^\circ\text{C}$ shown in Figure 12(b), it can be found that the optimization at the 1st initial resonance frequency obtains the highest 1st and the lowest 2nd resonance frequencies in the optimal design, and so does the optimiza-

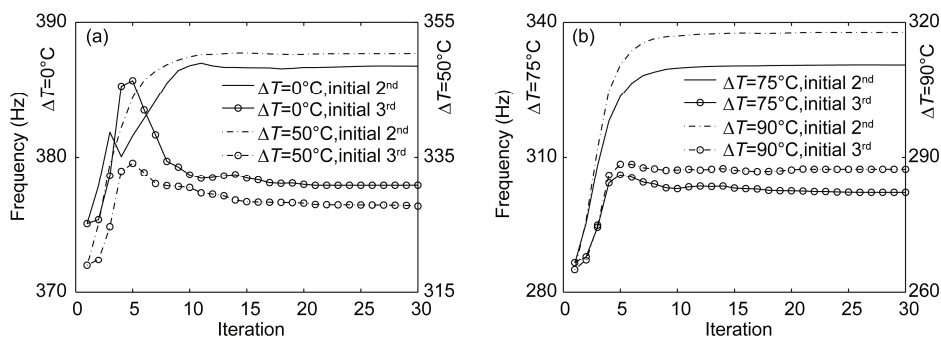


Figure 9 Iteration history of the order of the 2nd initial resonance frequency. (a) $\Delta T = 0, 50^\circ\text{C}$; (b) $\Delta T = 75, 90^\circ\text{C}$.

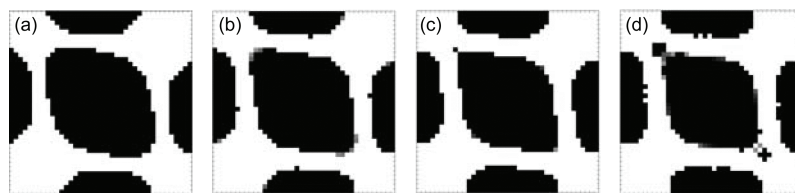


Figure 10 Optimal topology at the 1st and 2nd initial resonance frequencies (white - material 0, black- material 1). (a) $\Delta T = 0^\circ\text{C}$; (b) $\Delta T = 50^\circ\text{C}$; (c) $\Delta T = 75^\circ\text{C}$; (d) $\Delta T = 90^\circ\text{C}$.

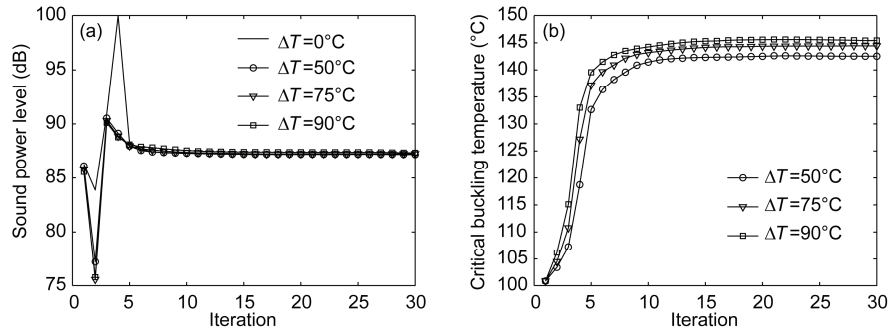


Figure 11 Iteration history of the radiated SPL and critical buckling temperature. (a) Radiated SPL; (b) critical buckling temperature.

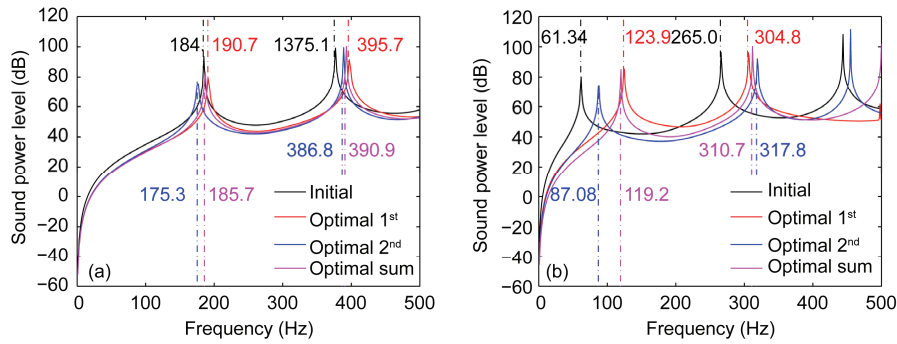


Figure 12 Radiated SPL in band 0–500 Hz of the initial and the optimal structures. (a) $\Delta T = 0^\circ\text{C}$; (b) $\Delta T = 90^\circ\text{C}$.

tion at the 2nd initial resonance frequency.

Figure 12 shows that the optimization improves the acoustic characteristics around the resonance frequencies except a narrow band, probably due to that the resonance response is much larger than the non-resonance response. Belegundu et al. [4] improved sound characteristics of a chain cover plate in the whole band, which demonstrated similar results to present work.

5.4 Optimization on SPL at the 13th initial resonance frequency

Figure 13 shows the optimal topology at the 13th initial resonance frequency, which is the highest frequency case investigated in this work. The material basically lumps according to the mode shape, similar to the topology obtained at the 1st or 2nd resonance frequency; as the mode shapes hardly vary in different thermal environments, topology almost stays unchanged.

Figures 14(a) and (b) show the iteration history of the radiated SPL and the 13th initial resonance frequency respectively; both exhibit similar changes to those obtained in the precious two subsections.

Figure 15 shows the iteration history of the critical buckling temperature.

Figure 16 shows that mode switching occurs during the optimization. Although it switches to the 12th at some iterations, the 13th initial mode stays the same order in the optimal design.

6 Conclusions

Topology optimization on radiated sound power at resonance frequencies in thermal environments is carried out in this paper, aiming at the improvement of acoustic characteristics in a frequency band. The dynamic response is obtained through a linear prestressed dynamic analysis fol-

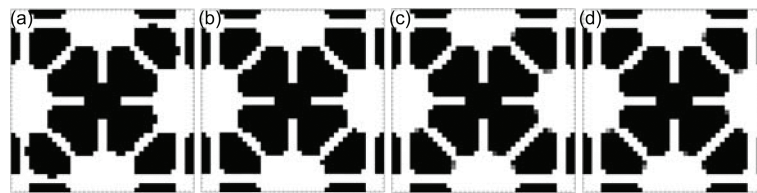


Figure 13 Topology at the 13th initial resonance frequency (white - material 0, black - material 1). (a) $\Delta T = 0^\circ\text{C}$; (b) $\Delta T = 50^\circ\text{C}$; (c) $\Delta T = 75^\circ\text{C}$; (d) $\Delta T = 90^\circ\text{C}$.

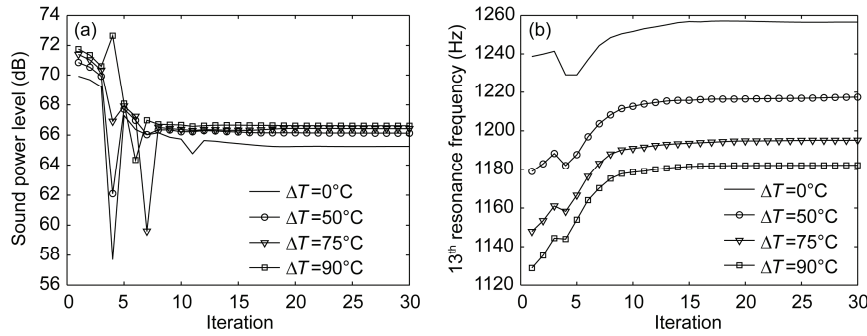


Figure 14 Iteration history of the radiated SPL, the 13th initial resonance frequency. (a) Radiated SPL; (b) 13th initial resonance frequency.

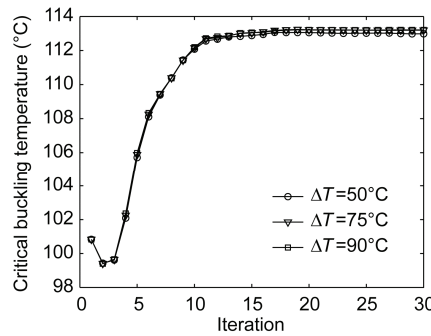


Figure 15 Iteration history of the critical buckling temperature.

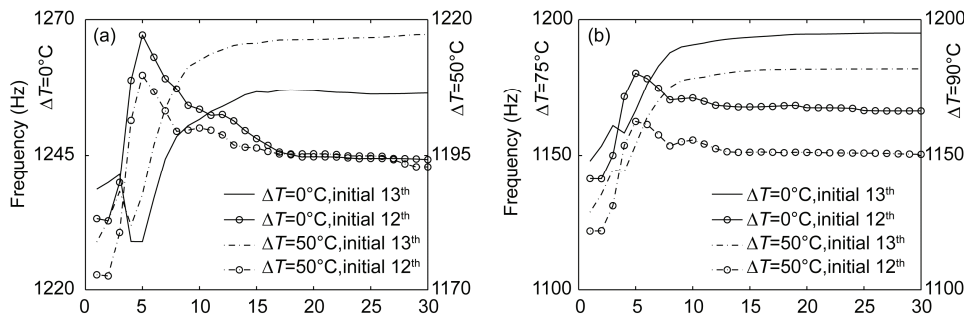


Figure 16 Iteration history of the order of the 13th initial resonance frequency. (a) $\Delta T = 0, 50^\circ\text{C}$; (b) $\Delta T = 75, 90^\circ\text{C}$.

lowing a thermal displacement calculation, and the radiated sound power is then calculated with Rayleigh integral. Adjoint method is employed in the sensitivity analysis, during which sensitivity of the resonance frequency is also considered.

Based on the numerical results, it could be concluded that the optimal topology is basically determined by the mode; since the mode shapes hardly change in different thermal environments, optimal topology shows similarity. As the temperature rises, the dynamic response becomes larger in higher thermal environment while the resonance frequency decreases, leading to an unobvious change of the radiated sound power. The optimization improves the acoustic characteristics around the resonance frequencies except a narrow range. The optimization results in gradually

growing resonance frequencies, indicating a stiffer structure. Mode switching could be observed, and mode tracking is adopted to ensure a smooth convergence. The critical buckling temperature increases as the optimization proceeds, indicating that the plate is always in the pre-buckling state.

This work was supported by the National Natural Science Foundation of China (Grant Nos. 11321062, 91016008 and 91216107). The assistance on the GCMMA algorithm from Prof. SVANBERG is gratefully acknowledged.

- 1 Heppenheimer T A. Facing the Heat Barrier: A History of Hypersonics. Washington DC: NASA History Series, 2007
- 2 Ma Z D, Hagiwara I. Sensitivity analysis methods for coupled acoustic-structural systems: Modal sensitivities. *AIAA J*, 1991, 29: 1787–1795

- 3 Ma Z D, Hagiwara I. Sensitivity analysis methods for coupled acoustic-structural systems: Direct frequency-response and its sensitivities. *AIAA J*, 1991, 29: 1796–1801
- 4 Belegundu A D, Salagame R R, Koopmann G H. A general optimization strategy for sound power minimization. *Struct Optim*, 1994, 8: 113–119
- 5 Hambric S A. Approximation techniques for broad-band acoustic radiated noise design optimization problems. *J Vib Acoust*, 1995, 117: 136–144
- 6 Kim N H, Dong J, Choi K K, et al. Design sensitivity analysis for a sequential structural-acoustic problems. *J Sound Vib*, 2003, 263: 569–591
- 7 Luo J H, Gea H G. Optimal stiffener design for interior sound reduction using a topology optimization based approach. *J Sound Vib*, 2003, 125: 267–273
- 8 Lee J, Wang S Y, Dikec A. Topology optimization for the radiation and scattering of sound from thin-body using genetic algorithms. *J Sound Vib*, 2004, 276: 899–918
- 9 Yoon G H, Jensen J S, Sigmund O. Topology optimization of acoustic-structure interaction problems using a mixed finite element formulation. *Int J Numer Meth Eng*, 2007, 70: 1049–1075
- 10 Du J, Olhoff N. Minimization of sound radiation from vibrating bi-material structures using topology optimization. *Struct Multidisc Optim*, 2007, 33: 305–321
- 11 Du J, Olhoff N. Topological design of vibrating structures with respect to optimum sound pressure characteristics in a surrounding acoustic medium. *Struct Multidisc Optim*, 2010, 42: 43–54
- 12 Penmetsa R C, Grandhi R V. Topology optimization for an evolutionary design of a thermal protection system. *AIAA J*, 2006, 44: 2663–2671
- 13 Manickarajah D, Xie Y M, Steven G P. An evolutionary method for optimization of plate buckling resistance. *Finite Elem Anal Des*, 1998, 29: 205–230
- 14 Foldaer J P, Hansen J S, Olhoff N. Optimization of the buckling load for composite structures taking thermal effects into account. *Struct Multidisc Optim*, 2001, 21: 14–31
- 15 Pedersen N L. On topology optimization of plates with prestress. *Int J Numer Meth Eng*, 2001, 51: 225–239
- 16 Pedersen N L. Topology optimization of laminated plates with prestress. *Comput Struct*, 2002, 80: 559–570
- 17 Lund E. Buckling topology optimization of laminated multi-material composite shell structures. *Compos Struct*, 2009, 91: 158–167
- 18 Yang X W, Chen G, Li Y M. Topology optimization of a bi-material material plate with respect to sound radiation in a thermal environment. *Int J Aerospace Lightweight Struct*, 2012, 2: 87–102
- 19 Yang X W, Li Y M. Topology optimization to minimize the dynamic compliance of a bi-material plate in a thermal environment. *Struct Multidisc Optim*, 2013, 47: 399–408
- 20 Yang X W, Chen G, Li Y M. Topological sensitivity analysis of structural sound radiation in a thermal environment. *Int J Aerospace Lightweight Struct*, 2012, 2: 365–382
- 21 Yang X W, Li Y M. Structural topology optimization on dynamic compliance at resonance frequency in thermal environments. *Struct Multidisc Optim*, 2014, 49: 81–91
- 22 Cook R D, Malkus D S, Plesha M E. *Concepts and Application of Finite Element Analysis*. 3rd ed. New York: John Wiley and Sons, 1989
- 23 Gao T, Zhang W H. Topology optimization involving thermo-elastic stress loads. *Struct Multidisc Optim*, 2010, 42: 725–738
- 24 Pan L, Lau G K, Du H, et al. On optimal design of HDD suspension using topology optimization. *Microsyst Technol*, 2002, 9: 137–146
- 25 Ewins D J. *Modal Testing: Theory and Practice*. London: Research Studies Press, 1984
- 26 Seyranian A P, Lund E, Olhoff N. Multiple eigenvalues in structural optimization problems. *Struct Optim*, 1994, 8: 207–227
- 27 Yang X Y, Xie Y M, Steven G P, et al. Topology optimization for frequencies using an evolutionary method. *J Struct Eng*, 1999, 125: 1432–1438
- 28 Svanberg K. A Globally Convergent Version of MMA Without Line Search. *First World Congress of Structural and Multidisciplinary Optimization*. Oxford: Pergamon, 1995. 9–16
- 29 Stolpe M, Svanberg K. An alternative interpolation scheme for minimum compliance topology optimization. *Struct Multidisc Optim*, 2001, 22: 116–124
- 30 Bendson M P, Sigmund O. *Topology Optimization, Theory, Methods and Applications*. Berlin: Springer, 2003